Wave Motion 49 (2012) 221–237

Contents lists available at SciVerse ScienceDirect

Wave Motion

journal homepage: www.elsevier.com/locate/wavemoti

On weakly nonlinear gravity–capillary solitary waves

Boguk Kim [a,*], Frédéric Dias [b], Paul A. Milewski [c]

[a] Pohang Mathematics Institute, POSTECH, Pohang, Gyungbuk, 790-784, Republic of Korea
[b] Centre de Mathématiques et de Leurs Applications, ENS Cachan, 94235 Cachan, France
[c] Department of Mathematics, UW-Madison, WI 53706-1388, USA

ARTICLE INFO

Article history:
Received 20 December 2010
Received in revised form 14 September 2011
Accepted 31 October 2011
Available online 7 November 2011

Keywords:
Euler equations
Gravity–capillary solitary waves
Weak nonlinearity
Zakharov's canonical variables
Dirichlet–Neumann operator
Cubic-order truncation model

ABSTRACT

As a weakly nonlinear model equations system for gravity–capillary waves on the surface of a potential fluid flow, a cubic-order truncation model is presented, which is derived from the ordinary Taylor series expansion for the free boundary conditions of the Euler equations with respect to the velocity potential and the surface elevation. We assert that this model is the optimal reduced simplified model for weakly nonlinear gravity–capillary solitary waves mainly because the generation mechanism of weakly nonlinear gravity–capillary solitary waves from this model is consistent with that of the full Euler equations, both quantitatively and qualitatively, up to the third order in amplitude.

In order to justify our assertion, we show that this weakly nonlinear model in deep water allows gravity–capillary solitary wavepackets in the weakly nonlinear and narrow bandwidth regime where the classical nonlinear Schrödinger (NLS) equation governs; this NLS equation derived from the model is identical to the one directly derived from the Euler equations. We verify that both quantitative and qualitative properties of the gravity–capillary solitary waves of the model precisely agree with the counterparts of the Euler equations near the bifurcation point by performing a numerical continuation to find the steady profiles of weakly nonlinear gravity–capillary solitary waves of the primary stable bifurcation branch. In addition, unsteady numerical simulations, in which those solitary waves are used as initial conditions, are provided as supporting evidences.

1. Introduction

Gravity–capillary solitary waves arise on the surface of an irrotational water flow at the finite length scale where the surface tension balances the gravitational force. In contrast to the well-known Korteweg–de Vries (KdV)-type solitary waves, of which steady wave profiles are expressed by sech^2 in the weakly nonlinear and long-wave limit, gravity–capillary solitary waves are known to bifurcated in the form of wavepackets with a nonzero carrier wavenumber, at which the linear phase speed is minimized, below the minimum phase speed. The KdV-type solitary waves bifurcate only when $B = 0$ or $B > \frac{1}{3}$; $B = \frac{\gamma}{\rho g h^2}$ is the Bond number, where γ is the surface tension coefficient, ρ is the fluid density, g is the gravitational acceleration, and h is the fluid depth. On the other hand, gravity–capillary solitary waves are possible only when the Bond number is less then $\frac{1}{3}$, including zero at infinite depth, in other words, in deep water.

The first discovery of gravity–capillary solitary waves is attributed to Longuet-Higgins [1] through his analytical result. He observed that there exists a certain length scale regime for which a surface tension may play a significant role to balance the gravitational acceleration even when the Bond number vanishes in the infinite-depth or small surface tension limit. In that sense, gravity–capillary solitary waves are clearly distinguished from the pure gravity counterparts in deep water.

* Corresponding author. Tel.: +82 10 7191 9717.
E-mail addresses: kimboguk@postech.ac.kr, kim.boguk@gmail.com (B. Kim).

0165-2125/$ – see front matter
doi:10.1016/j.wavemoti.2011.10.002

After Longuet-Higgins [2] computed the numerical profiles of the stable depression branch of gravity–capillary solitary waves from the full Euler equations, using a novel spectral method, thorough studies followed by other groups. Vanden-Broeck and Dias [3] performed an extensive numerical computation to find the complete bifurcation diagram of gravity–capillary solitary waves in deep water, using Cauchy's integral formula that expresses solutions in terms of the potential and stream functions. The generation mechanism of the gravity–capillary solitary waves in the form of weakly nonlinear wavepackets of nonlinear Schrödinger (NLS) type was identified by Longuet-Higgins [4], by Akylas [5], and by Dias and Iooss [6].

Afterward, more comprehensive numerical computations in arbitrary finite depths to compute the elevation and depression branches, as well as the turning points of the bifurcation diagram, were conducted for surface gravity–capillary solitary waves [7] and for interfacial gravity–capillary solitary waves [8]. The longitudinal stability, which is referred to as a stability property under disturbances only in the direction of wave propagations, of the gravity–capillary solitary waves was studied by Calvo and Akylas [9], along with the stability property of an associated forced problem. In their paper, they showed that depression solitary waves are stable and the elevation ones unstable.

Experimental realizations of gravity–capillary solitary waves on the surface of potential flows were made by Zhang and Longuet-Higgins. Zhang [10] observed solitary-like gravity–capillary waves in a wind wave tank, the depth of which is essentially deep in comparison with the short surface wavelength scale. A more elaborate comparison between experimental observations and earlier theoretical results on gravity–capillary solitary waves was done by Longuet-Higgins and Zhang [11]. In Zhang's later experiment [12], three-dimensional surface gravity–capillary waves were observed; however, those were thought of as nonlocal solitary waves rather than fully localized lump-type solitary waves.

It is more recent that three-dimensional fully locally confined solitary waves, referred to as gravity–capillary lumps, have been theoretically discovered by three different groups in the same physical condition. Părău, Vanden-Broeck, and Cooker computed the numerical profiles of steady gravity–capillary lumps from the full three-dimensional Euler equations, first in deep water [13], and then in finite depth [14], through their consecutive studies that use the boundary integral method. Milewski [15] also computed the numerical profiles of steady gravity–capillary lumps by using the Fourier spectral method, where a sech-type wave profile was taken as an initial guess for his numerical continuation, the formulation of which contains an extra virtual forcing parameter. It is important to notice that this discovery of fully localized gravity–capillary lumps in deep water does not conflict with Craig's nonexistence of lump-type solitary-wave solutions for pure gravity waves on the surface of deep water [16], although the relative surface tension effect on the gravitational force vanishes because the surface tension term has the highest order of derivatives in the dynamic boundary condition of the governing nonlinear partial differential equations.

Independently from the former two groups, Kim and Akylas [17] identified the generation mechanism of the gravity–capillary lumps in the weakly nonlinear limit. They verified that weakly nonlinear gravity–capillary solitary-wavepacket lumps bifurcate below the minimum phase speed with a carrier wavenumber at which the phase speed is minimized, in the same way as that of the weakly nonlinear plane gravity–capillary solitary-wave counterparts. In particular, they distinguished the finite-depth case and the deep-water one. In finite depth, those weakly nonlinear gravity–capillary solitary wavepackets are governed by the Benney–Roskes–Davey–Stewartson (BRDS) equations of elliptic–elliptic type, which were derived by Djordjevic and Redekopp [18] (a typographical mistake there has been pointed out by Ablowitz and Segur [19]). Those equations are simplified to the classical NLS equation in infinite depth.

In order to compute the numerical profiles of weakly nonlinear gravity–capillary solitary wavepackets, Kim and Akylas [17] combined a perturbation method and a pseudo-spectral numerical method that uses rational Chebyshev polynomials over the unbounded two-dimensional infinite domain. In that way, it was possible to effectively capture the slowly decaying tails of solitary waves in the far field, which become significant owing to the nontrivial leading-order meanflow effect, especially on the water of finite depth, as was asymptotically predicted by Akylas et al. [20].

In the same physical setting, it was shown that plane gravity–capillary solitary waves are unstable under long-wave disturbances in the transverse direction to the dominant solitary-wave propagation [21], using a perturbation method that is similar to the one used in the earlier studies by Kataoka and Tsutahara [22,23] and by Kataoka [24,25]. A similar result in the weakly nonlinear long-wave model equation for interfacial gravity–capillary solitary waves was provided by Kim and Akylas [26], and the generalized result for interfacial gravity–capillary solitary waves was provided by Kim [27]. The commonly verified transverse instability criterion is consistent with an earlier result by Bridges [28] for general water-wave problems.

Kim and Akylas [21] also asserted that the long-wave transverse instability of plane solitary waves must be related to the existence of the associated lump-type solitary waves: the former serves as a dynamic generation mechanism of gravity–capillary lumps. This statement was supported by the same authors' analytical and numerical results on long-wave interfacial gravity–capillary solitary waves based on the two-dimensional Benjamin (2-DB) equation [26].

In the context of the full Euler equations, however, the formation of gravity–capillary lumps via the long-wave transverse instability of the associated plane gravity–capillary solitary waves has not been truly justified yet with satisfactory numerical accuracy, although such a possibility was qualitatively indicated from some recent unsteady numerical computations for the dynamics of gravity–capillary solitary waves by Akers and Milewski on the basis of two-dimensional model equations [29,30]. In fact, highly accurate two-dimensional full Euler calculations of gravity–capillary solitary waves were only recently achieved via a conformal mapping technique by Milewski et al. [31]. It is regarded that the fully nonlinear numerical computation of the three-dimensional Euler equations, which is also suggested by Părău et al. [32], is still overly expensive,

considering that very precise numerical approximation at the singular point of the integral kernel is required. Accordingly, it is definitely beneficial to work with a more precise and efficient model under additional minimal assumptions in order to describe dynamics related with such dimension-breaking phenomena.

In principle, gravity–capillary solitary waves cannot be properly described by any long-wave models in a quantitatively accurate way, because their bifurcation occurs at a nonzero wavenumber in the weakly nonlinear limit. Instead, it is anticipated that some weakly nonlinear asymptotic models systematically derived from the original governing equations, not necessarily under any long-wave assumptions, should be able to capture significant dynamic properties – quantitative as well as qualitative – of gravity–capillary solitary waves.

In this study, therefore, the cubic-order truncation model of the Taylor series expansion of the free surface boundary conditions in the three-dimensional full Euler equations is proposed as an appropriate reduced model equations system for weakly nonlinear gravity–capillary solitary waves. This cubic-order weakly nonlinear truncation model, which is derived from the Hamiltonian formulation in terms of Zakharov's canonical variables with respect to the surface elevation and the value of the potential function on the free surface (see [33]), was introduced by Dyachenko et al. [34] in the study of the weak turbulent Kolmogorov spectrum of surface gravity waves.

When the free surface boundary conditions are represented in terms of Zakharov's canonical variables, one of the most important terms is the Dirichlet–Neumann operator (DNO). Generally speaking, the DNO gives a relation between the boundary value and the normal derivative of the harmonic function. This relation, in the Euler equations for potential flows, is naturally expressed in terms of Cauchy-type singular integrals which are analytic with respect to the weak surface elevation and the small variation of the domain geometry. In two spatial dimensions, the DNO is expressed by a uniformly convergent Taylor series (see [35,36]). Craig and Sulem [37] computed the uniformly convergent Taylor series of the DNO, in three dimensions, up to arbitrary orders, in their study of the dynamics of nonbreaking pure gravity waves on the surface of water in arbitrary finite depths.

This surface integral formulation that uses the DNO has been widely applied for various surface-wave problems since then. Nicholls [38] showed that this formulation can be effectively parallelized by implementing the numerical continuation to find steady surface wave profiles with the pseudo-spectral method. This method was later used to compute hexagonal periodic traveling surface wave structures [39,40]. Studies on variable bottom topographies with this formulation also have followed [41–43].

It is important to notice that the analyticity of the DNO, with respect to the variations of arbitrary smooth domain geometries, was mostly studied by Nicholls and Reitich [44–47]. They also showed that the ordinary perturbation procedure for the DNO, that is, the usual truncation of the Taylor series expansion, may be unstable and lose accuracy in high orders, but the convergence of the perturbation series for the DNO can be much enhanced by taking an alternative summation procedure such as the use of a Padé approximant (see also [48] for the analyticity of the DNO on doubly perturbed domains). However, such a numerical instability issue seems to be noticeable only when taking up to high-order perturbations, according to the numerical experiments reported by Nicholls and Reitich [47,49]. The low-order truncations of the series expansions are thought to be within a good approximation range as long as the wave amplitude is weak enough.

As inherent to the typical "boundary perturbation" method, classified by Nicholls [50], the issue about the uniform convergence of the series expansions for the free boundary conditions arises in other recursive algorithms. One is proposed by West et al. [51], in which they approximate the vertical derivative of the potential function at the free surface in terms of the series expansion with respect to the surface elevation. Another similar numerical model is developed by Dommermuth and Yue [52] for surface gravity waves, as well. However, Craig and Sulem [37] pointed out that both approaches are not known to be uniformly convergent for arbitrary wavenumbers. In fact, the former method is regarded to be consistent with respect to the order of the weak nonlinearity.

As an additional critical requirement for the ideal model equations system of weakly nonlinear gravity–capillary solitary waves, it is desired that the generation mechanism of gravity–capillary solitary-wave solutions should be *quantitatively equivalent* to what can be derived from the original Euler equations. This means that such model equations should allow the weakly nonlinear wavepackets of BRDS type – NLS type in deep water or in one spatial dimension – in the weakly nonlinear and narrow bandwidth limit, following exactly the same bifurcation mechanism from the original full Euler equations, not only qualitatively but also quantitatively. In this respect, we assert that the cubic-order truncation model of the Taylor series expansion for the free surface boundary conditions of the Euler equations should be the optimally efficient model for weakly nonlinear gravity–capillary solitary waves.

In the following sections, we justify our main assertion by deriving the NLS equation from the cubic-order truncation model, in which all of the coefficients in the NLS equation are identical to those directly derived from the full Euler equations. Moreover, we show that the numerically computed steady profiles of stable weakly nonlinear gravity–capillary solitary waves feature better quantitative agreement to the original ones from the full Euler equations than that from the NLS approximation. All these unsteady numerical computations are supported by some unsteady numerical simulations of stable solitary-wave propagations and their mutual interactions.

2. Weakly nonlinear cubic-order truncation model

Let us take $\sqrt{\gamma/(\rho g)}$ and $\left(\gamma/\left(\rho g^3\right)\right)^{1/4}$ as the length and time scales, respectively, where γ is the surface tension coefficient, g is the gravitational acceleration, and ρ is the constant fluid density. The flow is assumed to be irrotational. Then

the surface gravity–capillary waves in deep water are governed by the Euler equations for the velocity potential function $\phi(x, y, z, t)$ and the surface elevation $\eta(x, y, t)$ in the nondimensional form associated with the chosen length and time scales as follows:

$$\nabla^2\phi = 0 \quad \text{for } -\infty < z < \eta(x, y, t), \tag{1}$$

where $\nabla^2 \equiv \frac{\partial^2}{\partial x^2} + \frac{\partial^2}{\partial y^2} + \frac{\partial^2}{\partial z^2}$, with the kinematic boundary condition

$$\eta_t + \bar{\nabla}\eta \cdot \bar{\nabla}\phi = \phi_z \quad \text{for } z = \eta(x, y, t), \tag{2}$$

where $\bar{\nabla} \equiv \left(\frac{\partial}{\partial x}, \frac{\partial}{\partial y}\right)$, and with the dynamic boundary condition

$$\phi_t + \frac{1}{2}|\nabla\phi|^2 + \eta - \bar{\nabla} \cdot \frac{\bar{\nabla}\eta}{\sqrt{1 + |\bar{\nabla}\eta|^2}} = 0, \tag{3}$$

where $\nabla \equiv \left(\frac{\partial}{\partial x}, \frac{\partial}{\partial y}, \frac{\partial}{\partial z}\right)$, and with the far-field condition specified by

$$\nabla\phi \to 0 \quad \text{as } (|x|, |y|, |z|) \to +\infty. \tag{4}$$

(As is customary, the subscript variables denote partial differentiations.)

The kinematic and dynamic boundary conditions are expressed in terms of the value of the potential function $\zeta(x, y, t) = \phi(x, y, \eta(x, y, t), t)$ on the free surface $z = \eta(x, y, t)$, which are called Zakharov's canonical variables. Defining the DNO by

$$G[\eta]\{\zeta\} = \phi_z - \bar{\nabla}\eta \cdot \bar{\nabla}\phi = \sqrt{1 + |\bar{\nabla}\eta|^2}\, \frac{\partial\phi}{\partial\vec{n}}\bigg|_{z=\eta(x,y,t)}, \tag{5}$$

where $\vec{n}$ is the outward normal vector on the fluid surface, the kinematic and dynamic boundary conditions become

$$\eta_t = G[\eta]\{\zeta\}, \tag{6a}$$

$$\zeta_t = \frac{(G[\eta]\{\zeta\})^2 + 2\left(\bar{\nabla}\zeta \cdot \bar{\nabla}\eta\right) G[\eta]\{\zeta\} - \left(\zeta_x\eta_y - \zeta_y\eta_x\right)^2 - |\bar{\nabla}\zeta|^2}{2\left(1 + |\bar{\nabla}\eta|^2\right)} - \eta + \bar{\nabla} \cdot \frac{\bar{\nabla}\eta}{\sqrt{1 + |\bar{\nabla}\eta|^2}}. \tag{6b}$$

Under the assumption of the weak nonlinearity of Zakharov's canonical variables, the cubic-order truncation model of the Taylor series expansion of the free surface boundary conditions in the three-dimensional Euler equations is obtained by naturally extending from the two-dimensional results, as provided by Craig and Sulem [37] (see also [53]) in the following forms:

$$\eta_t - G_0\{\zeta\} = (G_1 + G_2)\{\zeta\}, \tag{7a}$$

$$\zeta_t + \eta - \bar{\nabla}^2\eta = \frac{1}{2}\left\{(G_0\{\zeta\})^2 - |\bar{\nabla}\zeta|^2\right\} - \left(G_0\{\eta G_0\{\zeta\}\} + \eta\bar{\nabla}^2\zeta\right) G_0\{\zeta\} - \frac{3}{2}|\bar{\nabla}\eta|^2\bar{\nabla}^2\eta + \eta_{xx}\eta_y^2 + \eta_{yy}\eta_x^2 - 2\eta_x\eta_y\eta_{xy}, \tag{7b}$$

where

$$G[\eta]\{\zeta\} = G_0\{\zeta\} + G_1\{\zeta\} + G_2\{\zeta\} + \cdots, \tag{8a}$$

$$G_0\{f\} = \int_{-\infty}^{+\infty}\int_{-\infty}^{+\infty}\sqrt{k^2 + l^2}\,\hat{f}(k, l, t)\mathrm{e}^{i(kx+ly-\omega t)}\mathrm{d}k\mathrm{d}l, \tag{8b}$$

$$\hat{f}(k, l, t) = \frac{1}{(2\pi)^2}\int_{-\infty}^{+\infty}\int_{-\infty}^{+\infty} f(x, y, t)\mathrm{e}^{-i(kx+ly-\omega t)}\mathrm{d}x\mathrm{d}y, \tag{8c}$$

$$G_1\{\zeta\} = -G_0\{\eta G_0\{\zeta\}\} - \bar{\nabla} \cdot \left(\eta\bar{\nabla}\zeta\right), \tag{8d}$$

$$G_2\{\zeta\} = \frac{1}{2}\bar{\nabla}^2\left(\eta^2 G_0\{\zeta\}\right) + \frac{1}{2}G_0\{\eta^2\bar{\nabla}^2\zeta\} + G_0\{\eta G_0\{\eta G_0\{\zeta\}\}\}, \tag{8e}$$

where $\bar{\nabla}^2 = \frac{\partial^2}{\partial x^2} + \frac{\partial^2}{\partial y^2}$.

3. Weakly nonlinear gravity–capillary solitary wavepackets

From (7), weakly nonlinear narrow-banded solitary wavepackets that bifurcate below the minimum phase speed are derived in the following forms, correct up to $O(\epsilon^3)$:

$$\eta(x, y, t) \approx \epsilon S_1(X, Y, T)E + \epsilon^2 S_0(X, Y, T) + \epsilon^2 S_2(X, Y, T)E^2 + \text{c.c.}, \tag{9a}$$

$$\zeta(x, y, t) \approx \epsilon A_1(X, Y, T)E + \epsilon A_0(X, Y, T) + \epsilon^2 A_2(X, Y, T)E^2 + \text{c.c.}, \tag{9b}$$

with

$$S_n = S_n^{(0)} + \epsilon S_n^{(1)} + \epsilon^2 S_n^{(2)} + O(\epsilon^3) + \cdots, \tag{10a}$$

$$A_n = A_n^{(0)} + \epsilon A_n^{(1)} + \epsilon^2 A_n^{(2)} + O(\epsilon^3) + \cdots, \tag{10b}$$

for all nonnegative integers n, and with

$$E = \mathrm{e}^{i(k_0 x + l_0 y - \omega_0 t)}, \tag{11a}$$

$$X = \epsilon \left(x - \left. \frac{\partial \omega}{\partial k} \right|_0 t \right), \tag{11b}$$

$$Y = \epsilon \left(y - \left. \frac{\partial \omega}{\partial l} \right|_0 t \right), \tag{11c}$$

$$T = \epsilon^2 t, \tag{11d}$$

$$\omega_0^2 = \kappa_0 \left(1 + \kappa_0^2\right) \quad \text{for } \kappa_0 = \sqrt{k_0^2 + l_0^2}, \tag{11e}$$

$$\epsilon \ll 1, \tag{11f}$$

where the phase speed is minimized at the wavenumber $(k_0, l_0) = (1, 0)$. The leading-order meanflow of the potential function is considered to be $O(\epsilon)$ but vanishes for gravity–capillary solitary waves in deep water. As a result, any coupling between the wave envelope of the primary harmonics and the meanflow is ineffective, so the leading-order wave envelope of the primary harmonics $S_1(X, Y, T)$ satisfies the NLS equation in deep water; otherwise, in any finite depths, $S_1(X, Y, T)$ and $A_{1X}(X, Y, T)$ satisfy the BRDS equations, coupled together.

A standard NLS, or equivalently BRDS, derivation procedure for weakly nonlinear solitary wavepackets of these forms described in (9)–(11) has been completely developed since the original contribution by Benney and Newell [54], in which the NLS equation was claimed to be a proper model equation in the water-wave problem. Hasimoto and Ono [55] clearly expressed the linear or nonlinear operators of multiple scales in terms of perturbation series in the derivation of the NLS equation for plane gravity wavepackets. Davey and Stewartson [56] "closely followed" the analysis of Hasimoto and Ono for the derivation of their two-dimensional model equation for three-dimensional surface gravity wavepackets, although all necessary computations for deriving the Davey–Stewartson equation were already introduced earlier by Benney and Roskes [57] in the discussion of wave instabilities for gravity waves (Davey and Stewartson extracted the single-equation form). Rigorous convergence analysis is discussed by Craig et al. [58] for surface gravity waves, and by Craig et al. [59] for surface gravity–capillary waves, respectively.

A key idea in the NLS derivation is that weakly nonlinear solitary-wave solutions are represented in terms of the Fourier integral in order to express individual linear operators in terms of perturbation expansions from

$$f(x, y, t) = E \int_{-\infty}^{+\infty} \int_{-\infty}^{+\infty} \hat{f}(k, l, t) \mathrm{e}^{i\{(k-k_0)x + (l-l_0)y - (\omega - \omega_0)t\}} \mathrm{d}k \mathrm{d}l. \tag{12}$$

As is described by Hogan's analysis [60] for his derivation of a fourth-order envelope equation for three-dimensional gravity–capillary wavepackets in deep water (a comprehensive review on this topic is found in [61]), we have

$$\begin{aligned} \omega - \omega_0 = {} & \left. \frac{\partial \omega}{\partial k} \right|_0 (k - k_0) + \left. \frac{\partial \omega}{\partial l} \right|_0 (l - l_0) + \frac{1}{2} \left. \frac{\partial^2 \omega}{\partial k^2} \right|_0 (k - k_0)^2 \\ & + \frac{1}{2} \left. \frac{\partial^2 \omega}{\partial l^2} \right|_0 (l - l_0)^2 + \left. \frac{\partial^2 \omega}{\partial k \partial l} \right|_0 (k - k_0)(l - l_0) + \cdots. \end{aligned} \tag{13}$$

Under the assumption that the Fourier spectrum is narrow banded in the same magnitude of the weak nonlinearity around the wavenumber (k_0, l_0), the following fast wavenumber variables are introduced by

$$K = \epsilon^{-1} (k - k_0), \qquad L = \epsilon^{-1} (l - l_0). \tag{14}$$

Then we have the general expression of a slowly varying modulated wavepacket, which is weakly deviated from a monochromatic traveling wave with the wavenumber k_0 and the frequency ω_0, regardless of any underlying physical principles, by

$$F(X, Y, T) \approx \int_{-\infty}^{+\infty} \int_{-\infty}^{+\infty} \hat{F}(K, L, T) \mathrm{e}^{i(KX + LY - \Omega T)} \mathrm{d}K \mathrm{d}L, \tag{15}$$

where

$$\hat{F}(K, L, T) = \epsilon^2 \hat{f} \left(k_0 + \epsilon K, l_0 + \epsilon L, \frac{T}{\epsilon^2} \right), \tag{16a}$$

$$\Omega = \frac{1}{2} \left. \frac{\partial^2 \omega}{\partial k^2} \right|_0 K^2 + \frac{1}{2} \left. \frac{\partial^2 \omega}{\partial l^2} \right|_0 L^2 + \left. \frac{\partial^2 \omega}{\partial k \partial l} \right|_0 KL. \tag{16b}$$

Therefore we obtain the perturbation expansions of the linear operators, which are applied to wavepackets of the primary harmonics, up to $O(\epsilon^2)$:

$$\frac{\partial}{\partial t} = -i\omega_0 - \epsilon\left(\left.\frac{\partial\omega}{\partial k}\right|_0\frac{\partial}{\partial X} + \left.\frac{\partial\omega}{\partial l}\right|_0\frac{\partial}{\partial Y}\right) + \epsilon^2\frac{\partial}{\partial T} + \cdots, \tag{17a}$$

$$G_0 \approx \sqrt{k_0^2+l_0^2} - \frac{i\epsilon}{\sqrt{k_0^2+l_0^2}}\left(k_0\frac{\partial}{\partial X} + l_0\frac{\partial}{\partial Y}\right) + \frac{\epsilon^2}{2\left(k_0^2+l_0^2\right)^{\frac{3}{2}}}\left(-l_0^2\frac{\partial^2}{\partial X^2} - k_0^2\frac{\partial^2}{\partial Y^2} + 2k_0l_0\frac{\partial^2}{\partial X\partial Y}\right), \tag{17b}$$

$$\frac{\partial}{\partial x} = ik_0 + \epsilon\frac{\partial}{\partial X}, \tag{17c}$$

$$\frac{\partial}{\partial y} = il_0 + \epsilon\frac{\partial}{\partial Y}. \tag{17d}$$

For wavepackets multiplied by the other high-order harmonics, the perturbation series for the linear operators can be defined in a similar way.

Since we derive a system of model equations for weakly nonlinear wavepackets at the third-order perturbations, perturbations to the linear operators at least up to second order are required in performing the perturbation procedure: fewer orders of perturbation expansions to the linear operators may lead to quantitatively inaccurate results unless a perturbation series stops at $O(\epsilon)$, although some qualitative properties may be captured in lower orders in a consistent manner. As usual, the leading-order perturbation equation is the linear dispersion relation, and the second-order perturbation equation implies that wavepackets move with the group velocity. Based on our particular choice of the ansatz here, both leading-order and second-order perturbation equations are trivially satisfied. It is clearly seen that the linear operator parts for the wavepackets of the primary harmonics, obtained by eliminating η from the dynamic boundary condition, first appear in $O\left(\epsilon^2\right)$ as follows:

$$\frac{\partial^2}{\partial t^2} + \left(1-\bar{\nabla}^2\right)G_0 \approx -\epsilon^2\omega_0\left(2i\frac{\partial}{\partial T} + \left.\frac{\partial^2\omega}{\partial k^2}\right|_0\frac{\partial^2}{\partial X^2} + \left.\frac{\partial^2\omega}{\partial l^2}\right|_0\frac{\partial^2}{\partial Y^2} + 2\left.\frac{\partial^2\omega}{\partial k\partial l}\right|_0\frac{\partial^2}{\partial X\partial Y}\right). \tag{18}$$

The expression on the right-hand side in (18) is obtained by computing the perturbation series of $\left(1-\bar{\nabla}^2\right)G_0$ from the Taylor series of ω^2 at (k_0, l_0) and then by collecting all of the $O(\epsilon^2)$ terms. The terms correct up to $O(\epsilon)$ are cancelled out with the terms from $\frac{\partial^2}{\partial t^2}$. In fact, this expression (18) is nothing but the linear operator for the NLS equation in the $O(\epsilon^3)$ terms for the weakly nonlinear wavepackets of which the magnitude is $O(\epsilon)$.

The perturbation procedure up to the third order is performed by collecting the zeroth and the second harmonic terms up to $O(\epsilon^2)$ and the primary harmonic terms up to $O(\epsilon^3)$ from the kinematic and dynamic boundary conditions. Taking into account all nonlinear terms, the coefficients precisely match the ones derived directly from the full Euler equations, without any further scaling. The resulting NLS equation is obtained by

$$\left\{i\frac{\partial}{\partial T} + \frac{1}{2}\left(\left.\frac{\partial^2\omega}{\partial k^2}\right|_0\frac{\partial^2}{\partial X^2} + \left.\frac{\partial^2\omega}{\partial l^2}\right|_0\frac{\partial^2}{\partial Y^2} + 2\left.\frac{\partial^2\omega}{\partial k\partial l}\right|_0\frac{\partial^2}{\partial X\partial Y}\right)\right\}S_1^{(0)} + \left\{\frac{2\kappa_0^2\omega_0^3}{\omega_2^2-4\omega_0^2} - \left(2\omega_0^2 - \frac{3}{2}\kappa_0^3\right)\frac{\kappa_0^2}{2\omega_0}\right\}\left|S_1^{(0)}\right|^2 S_1^{(0)} = 0. \tag{19}$$

It is noteworthy that the additional nonlinear term obtained from the cubic-order truncation over the quadratic-order truncation of the Taylor series expansion of the free surface boundary conditions is $\left(2\omega_0^2 - \frac{3}{2}\kappa_0^3\right)\frac{\kappa_0^2}{2\omega_0}\left|S_1^{(0)}\right|^2 S_1^{(0)}$. This means that the nonlinear effect in the normal stress balance on the surface of fluid is not precisely explained only by the quadratic truncation, because there is no contribution from the quadratic truncation to the nonlinear term of $O(\epsilon^3)$ in the dynamic boundary condition. This gives another reason why at least the third-order truncation terms are all required to describe the dynamics of slowly varying weakly nonlinear narrow-banded solitary wavepackets on the free surface of a fluid flow in a quantitatively proper way.

The NLS equation is particularly interesting at the phase speed minimizing wavenumber $(k_0, l_0) = (1, 0)$, for which the coefficients of NLS in (18) and (19) are computed by

$$\left.\frac{\partial\omega}{\partial k}\right|_0 = \sqrt{2}, \qquad \left.\frac{\partial\omega}{\partial l}\right|_0 = 0, \qquad \left.\frac{\partial^2\omega}{\partial k^2}\right|_0 = \frac{\sqrt{2}}{2}, \qquad \left.\frac{\partial^2\omega}{\partial l^2}\right|_0 = \sqrt{2}, \qquad \left.\frac{\partial^2\omega}{\partial k\partial l}\right|_0 = 0. \tag{20}$$

Therefore the NLS equation

$$iS_{1T}^{(0)} + \frac{\sqrt{2}}{4}S_{1XX}^{(0)} + \frac{\sqrt{2}}{2}S_{1YY}^{(0)} + \frac{11}{8}\sqrt{2}\left|S_1^{(0)}\right|^2 S_1^{(0)} = 0 \tag{21}$$

allows solitary-wavepacket solutions moving in the x-direction because the group velocity is equal to the phase velocity, which is $\sqrt{2}$, at the critical wavenumber. In two dimensions with one spatial variable, all coefficients of this NLS equation precisely agree with the earlier results [4–6]. In three dimensions with two spatial variables, this is consistent with the other earlier results [18,19] as confirmed by Kim and Akylas in two dimensions [21] and in three dimensions [17] for a different nondimensionalization with the same physical setting.

The coefficient of the cubic-order nonlinear term in (19) should be invariant either in two or three dimensions, even for wavepackets moving in oblique directions. In general, the group velocity and the phase velocity have different directions to each other. Even in such cases, solitary wavepackets arise when the projection of the group velocity onto the direction of the phase velocity coincides with the phase velocity itself.

In two dimensions, spatially with the X-dependence only, there are well-known fully localized solitary wave solutions. Letting

$$S_1^{(0)}(X,T) = S(X)\mathrm{e}^{i\alpha T}, \tag{22}$$

where α is an arbitrary positive real number, we have

$$S(X) = \sqrt{\frac{2\alpha}{\mu}}\,\mathrm{sech}\left(\sqrt{\frac{\alpha}{\beta}}X\right) \tag{23}$$

for

$$-\alpha S + \beta\frac{\partial^2 S}{\partial X^2} + \mu\,|S|^2 S = 0. \tag{24}$$

Hence, from (21), we have

$$\eta(x,t) \approx \tilde{\epsilon}\,\frac{2^{\frac{11}{4}}}{\sqrt{11}}\,\mathrm{sech}\left\{2^{\frac{3}{4}}\tilde{\epsilon}\left(x-\sqrt{2}t\right)\right\}\cos\left(x-\sqrt{2}t-x_0\right), \tag{25a}$$

$$\zeta(x,t) \approx \tilde{\epsilon}\,\frac{2^{\frac{13}{4}}}{\sqrt{11}}\,\mathrm{sech}\left\{2^{\frac{3}{4}}\tilde{\epsilon}\left(x-\sqrt{2}t\right)\right\}\sin\left(x-\sqrt{2}t-x_0\right), \tag{25b}$$

up to $O(\tilde{\epsilon}^3)$, where $\tilde{\epsilon} = \epsilon\sqrt{\alpha}$ and x_0 is an arbitrary phase. Since α is arbitrary, the above expressions are valid as long as $\tilde{\epsilon} \ll 1$. It is important to mention that the gravity–capillary surface solitary waves are known to be stable for $x_0 = \pi$ (depression) and unstable for $x_0 = 0$ (elevation).

4. Weakly nonlinear gravity–capillary solitary waves

4.1. Steady computation

The solitary-wave solutions of the cubic-order truncation model are computed by numerical continuation that uses the Moore–Penrose inverse with arc-length parameterization. The application of this method for the computation of steady surface-wave solutions has been discussed earlier by Nicholls [38].

The bifurcation diagram for depression gravity–capillary solitary waves is plotted in Fig. 1. The pseudo-spectral method is used with a domain-stretching transformation, as was used by Kim and Akylas [17,21,26] for the numerical computation of steady gravity–capillary solitary waves: for the stretching parameter, $L = 16$ is taken for the Euler equations, and $L = 80$ for the cubic-order truncation model. For the number of discretization points, $N = 512$ is chosen. See [21] for the convergence of the method with respect to the number of discretization points. The details on computing the gravity–capillary solitary waves in deep water from the Euler equations based on this numerical method are summarized in the Appendix.

For the Euler equations, the (longitudinal) stability of gravity–capillary solitary waves was verified by Calvo and Akylas [9]. Near the bifurcation point, the quantitative agreement between the cubic-order truncation model and the Euler equations is fairly good. When the solitary wave speed is far below the bifurcation wave speed $V_0 = \sqrt{2}$, however, the cubic-order truncation model is no longer a good approximation to the Euler equations: the separation between the bifurcation curves is apparent when the solitary wave speed is less than 1.35, approximately, particularly for the steepness of the potential function on the surface (see Fig. 1). This gives the valid regime of the wave amplitude scale in which the weakly nonlinear cubic-order truncation model works quantitatively close to the Euler equations.

The steady solitary-wave profiles are compared in Fig. 2 for $V = \sqrt{2} - 0.01$, in Fig. 3 for $V = \sqrt{2} - 0.04$, and in Fig. 4 for $V = 1.35$. In comparison of the numerical steady solitary-wave solution profiles, the cubic-order truncation model and the Euler equations are seemingly indistinguishable each other.

The magnitudes of the Fourier spectra of weakly nonlinear gravity–capillary solitary waves are plotted in Fig. 5 for the surface elevation and the derivative of the surface potential function, both of which are even, from the cubic-order truncation model. Near the bifurcation point when $V = \sqrt{2}$, the highest peak of the magnitudes of Fourier spectra is attained at the

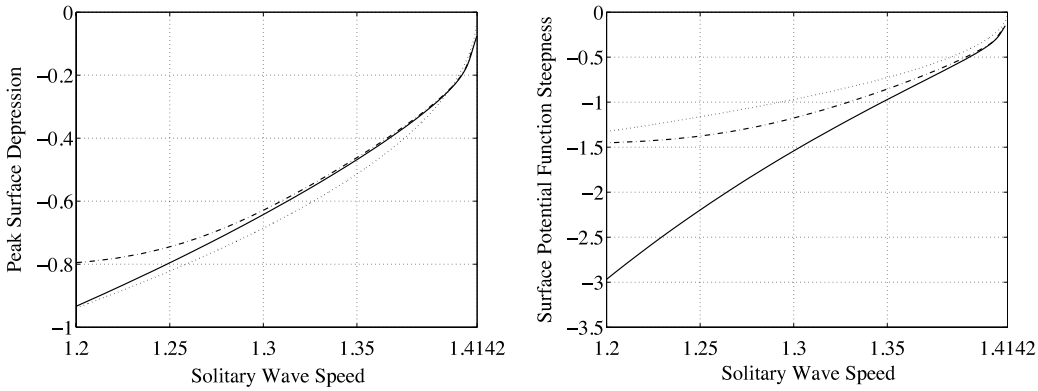

Fig. 1. The bifurcation diagram for the branch of depression solitary waves. The peak surface depression, $\eta|_{\xi=0}$, (left) and the steepness of the potential function on the surface, $\mathrm{d}\zeta/\mathrm{d}\xi|_{\xi=0}$, (right) for the NLS model $(-\cdot-)$, the Euler model $(-)$, and the cubic-order truncation model $(--)$, where $\xi = x - Vt$. The cubic-order truncation model becomes a very precise approximation to the Euler equations when the solitary wave speed, denoted by V, is sufficiently close to the bifurcation point $\sqrt{2}$. Near the bifurcation point, moreover, the bifurcation curve of the cubic-order truncation model resolves the sharp change of the Euler equations counterpart, whereas the NLS model does not. Below $V = 1.35$, the deviation of the model equations for the steepness of the surface potential function from the Euler equations is relatively greater than that of the peak surface depression.

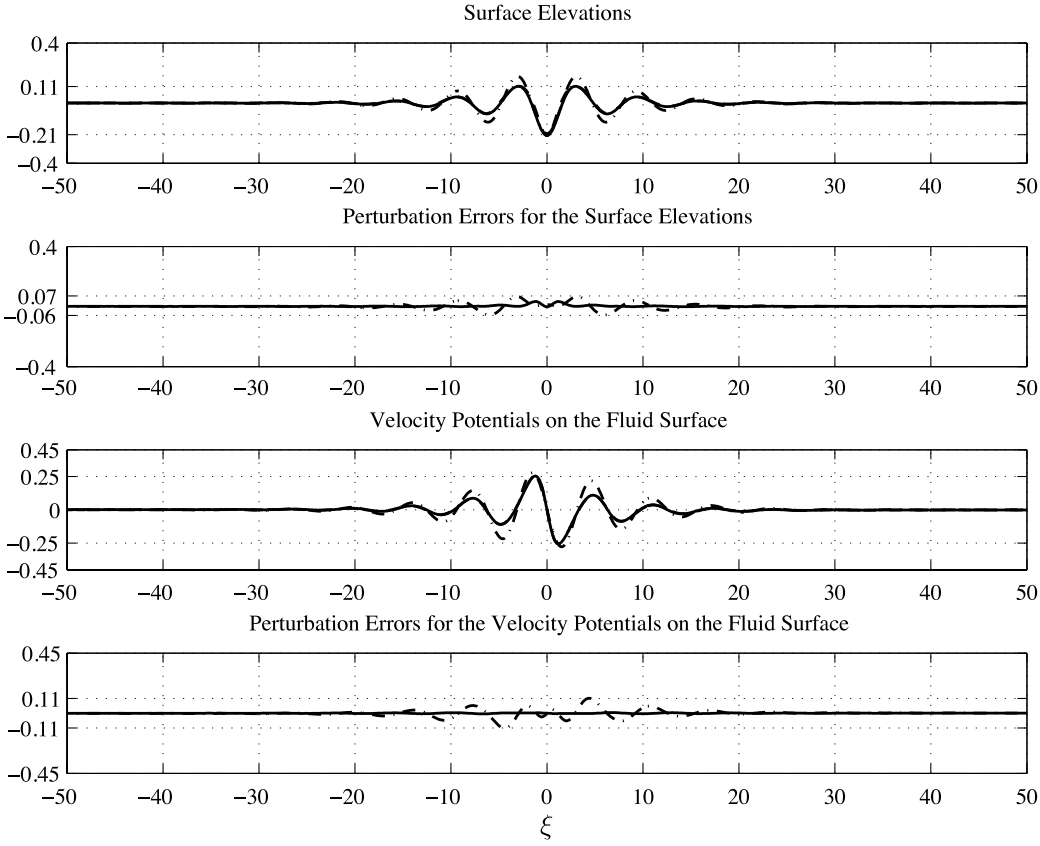

Fig. 2. Comparison of gravity–capillary solitary wave solutions near the bifurcation point below the minimum of phase speed at the carrier wavenumber $k_0 = 1$ for the solitary wave speed $V = \sqrt{2-\epsilon^2}$ when $\epsilon = 0.1$: NLS model $(-\cdot-)$, Euler model $(-)$, and the cubic-order truncation model $(--)$ in the first and the third figures; perturbation errors between the cubic-order truncation model and the Euler model $(-)$ and between the NLS model and the Euler model $(-\cdot-)$ in the second and the fourth figures, respectively. The cubic-order truncation model shows a better agreement with the Euler equations than with the NLS model.

carrier wavenumber $k_0 = 1$ of the primary harmonics of the solitary wavepacket and the second peak at the wavenumber of the second harmonics. As expected, the Fourier spectra become more broadened as the solitary wave speed goes farther away from the bifurcation wave speed. It is also interesting to note that the magnitudes of the peak Fourier coefficients are similar regardless of the solitary wave speed.

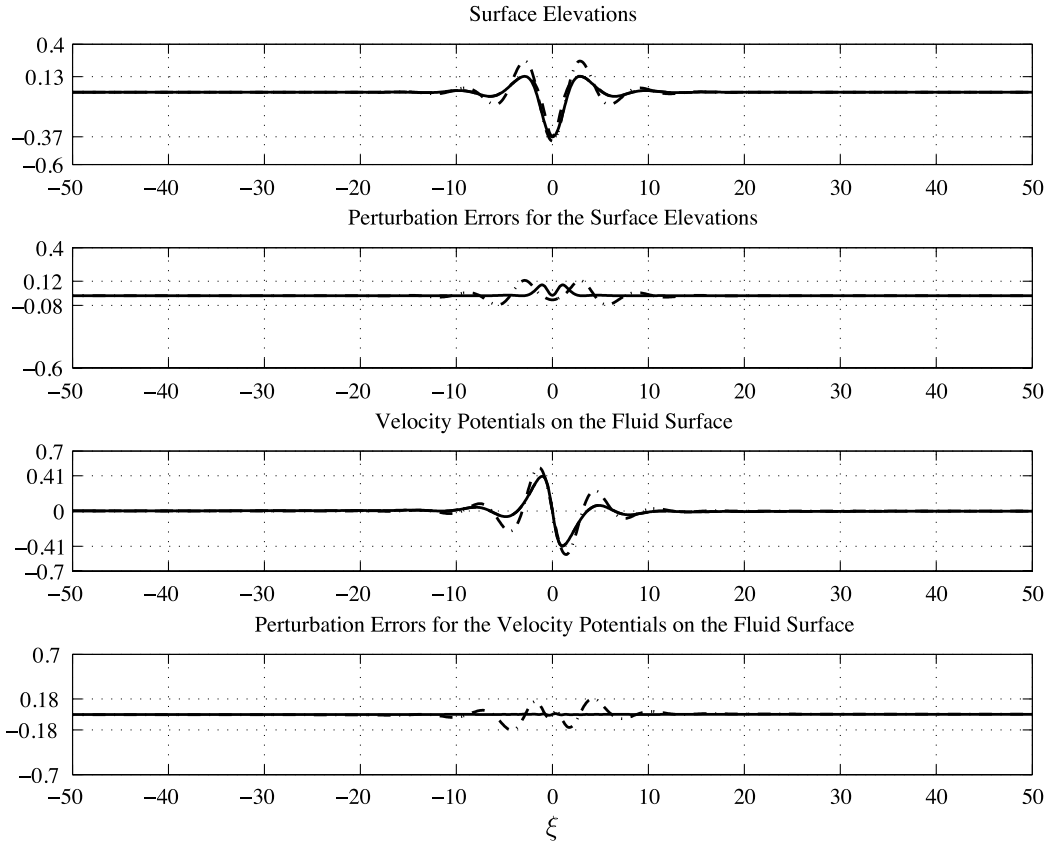

Fig. 3. Comparison of gravity–capillary solitary wave solutions near the bifurcation point below the minimum of phase speed at the carrier wavenumber $k_0 = 1$ for the solitary wave speed $V = \sqrt{2}-\epsilon^2$ when $\epsilon = 0.2$: NLS model ($-\cdot-$), Euler model ($-$), and the cubic-order truncation model ($--$) in the first and the third figures; perturbation errors between the cubic-order truncation model and the Euler model ($-$) and between the NLS model and the Euler model ($-\cdot-$) in the second and the fourth figures, respectively. The profiles of solitary waves have losing wavepacket properties, but the solitary-wave profiles from the cubic-order truncation model still seem hardly distinguishable from the counterparts of the Euler equations. Quantitative discrepancies between NLS and Euler are apparently noticeable.

4.2. Unsteady simulations

The unsteady numerical simulations are presented by combining the Fourier spectral method with the explicit Runge–Kutta fourth-order method under the application of the integrating factor (see [62] for the implementation idea). For the spatial discretization size, $\Delta x = 0.1$ is used.

In Figs. 6–8, the weakly nonlinear gravity–capillary solitary waves of the cubic-order truncation mode for $V = \sqrt{2}-0.01$, $V = \sqrt{2} - 0.04$, and $V = 1.35$ are taken as the initial conditions, respectively, for the common discretized time step $\Delta t = 0.005$. Note that the shapes of the weakly nonlinear gravity–capillary solitary waves are stably maintained for 100 nondimensional time units for each case. However, when the solitary wave speed is less than 1.305, such that the nonlinearity becomes stronger, the numerically computed steady profiles of weakly nonlinear gravity–capillary solitary waves are not stable in the cubic-order truncation model.

In Fig. 9, a dynamic interaction between weakly nonlinear gravity–capillary solitary waves for $V = \sqrt{2} - (0.1)^2$ and $V = \sqrt{2} - (0.2)^2$ is presented for 2000 nondimensional time units with $\Delta t = 0.001$. The former gravity–capillary solitary wave is smaller and faster, so it collides with the latter larger and slower one. After the interaction, each of them is separated out again as another solitary wave. The larger one is slowed down, with the new approximate wave speed 1.3708, and its amplitude becomes slightly higher; the smaller one becomes even smaller and faster. This features an inelastic solitary wave collision because each shape is not maintained to be the initial one, which is typical to any nonintegrable dynamical system.

5. Discussion and conclusion

In the sense of weak nonlinearity, this cubic-order truncation model equations system is regarded as a quantitatively precise and optimally efficient reduced model for gravity–capillary waves for the following reasons. First, only the weak

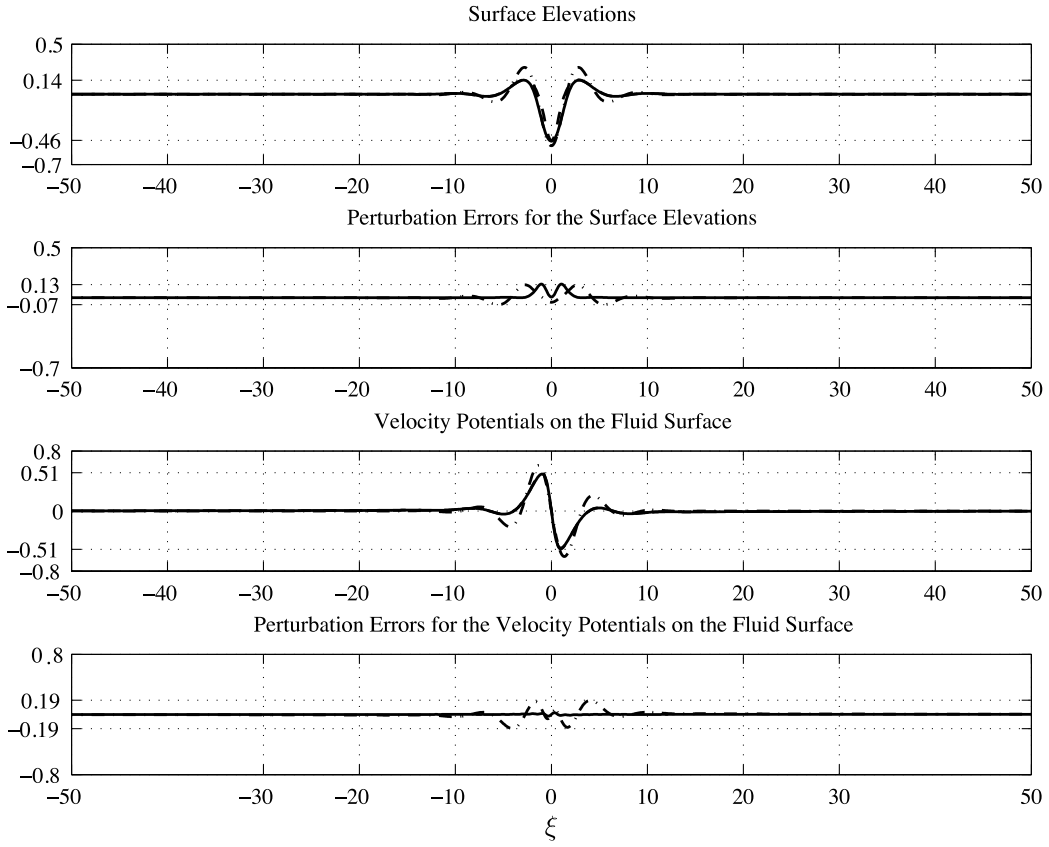

Fig. 4. Comparison of gravity–capillary solitary wave solutions below the minimum of phase speed at the carrier wavenumber $k_0 = 1$ for the solitary wave speed $V = 1.35$ ($\epsilon \approx 0.253$), where $\xi = x - Vt$: NLS model ($- \cdot -$), Euler model ($-$), and the cubic-order truncation model ($- -$) in the first and the third figures; perturbation errors between the cubic-order truncation model and the Euler model ($-$) and between the NLS model and the Euler model ($- \cdot -$) in the second and the fourth figures, respectively. The perturbation errors for both the cubic-order truncation model and NLS from Euler become larger as the nonlinearity is stronger.

nonlinearity of Zakharov's canonical variables is assumed. Second, the classical NLS equation, derived from them, takes exactly the same form as the one derived from the full Euler equations, not requiring any further scaling. Third, more qualitative and quantitative properties of the gravity–capillary solitary waves of the original full Euler equations are better explained, such as the profiles of gravity–capillary solitary wave solutions, the bifurcation diagrams near the bifurcation point, and the nonlinear effect of the normal stress balance on the surface.

The quantitatively consistent skew-symmetric property of the associated linearized operators can be shown in the order of the wave amplitudes under the assumption of weak nonlinearity, from which the long-wave transverse instability of weakly nonlinear gravity–capillary solitary waves can be directly derived [63]. This indicates that it will be possible to perform accurate numerical computations for the steady profiles of weakly nonlinear gravity–capillary lumps and the dynamic generation of such lump-type solitary waves via the long-wave transverse instability of the weakly nonlinear gravity–capillary solitary waves, similarly as observed in the numerical simulations of the earlier studies [17,21,26].

Acknowledgments

The authors wish to thank Prof. T.R. Akylas for his helpful comments in clarifying a particular meaning of this model equations system in the quantitative perspective. This paper was partially supported by the French Agence Nationale de la Recherche project MANUREVA ANR-08-SYSC-019 and by Priority Research Centers Program through the National Research Foundation of Korea (NRF) grant funded by the Ministry of Education, Science and Technology of the Korean government (2010-0029638). PAM wishes to thank the CNRS for sponsoring his visit to Ecole Normale Supérieure de Cachan in 2008 2009, the NSF for support under Grant DMS-0908077, and the EPSRC for support under Grant Number GR/S47786/01.

Appendix A. Cauchy's integral formula for the two-dimensional potential flow in infinite depth

In this Appendix, a formulation is presented to compute surface gravity–capillary solitary-wave solutions in two spatial dimensions from the potential flow assumption, which uses Cauchy's integral formula with respect to the potential and

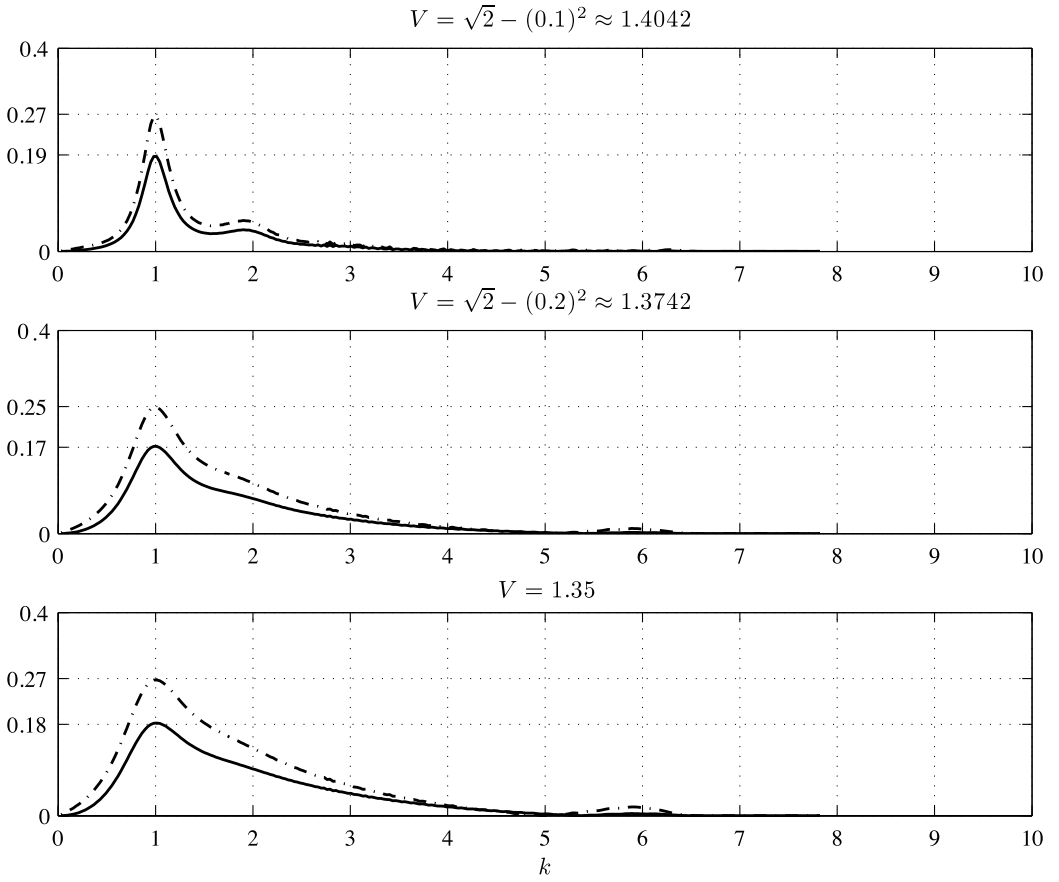

Fig. 5. The magnitudes of the Fourier spectral of gravity–capillary solitary waves from the cubic-order truncation model at the solitary wave speed $V = \sqrt{2} - 0.01$, $\sqrt{2} - 0.04$, and 1.35: $|\mathcal{F}\{\eta(\xi)\}(k)|$ $(-)$ and $|\mathcal{F}\{\zeta(\xi)\}(k)|$ $(-\cdot-)$, where $\xi = x - Vt$. As the solitary waves appear farther away from the bifurcation point, the associated Fourier spectra are broadened.

stream functions, originally developed by Vanden-Broeck and Dias [3]. The same formulation was used in later studies to compute surface gravity–capillary solitary waves in arbitrary finite depth [7] and interfacial gravity–capillary solitary waves [8]. The same method was used to reproduce the earlier results by Calvo and Akylas [9,64] and by Kim and Akylas [21]. This formulation was recently implemented by Milewski et al. [31] to compute the initial conditions for dynamic computations of plane gravity–capillary waves.

Particularly in this study, the computation of various conserved quantities for gravity–capillary solitary waves is highlighted. See [65,66] for similar discussions in terms of the potential and stream functions, which was also addressed by Kim and Akylas [21].

Let us consider gravity–capillary solitary waves from the following water-wave problem in deep water, which is described by the full Euler equations in two spatial dimensions:

$$\frac{\partial^2 \bar{\phi}}{\partial \xi^2} + \frac{\partial^2 \bar{\phi}}{\partial z^2} = 0 \quad \text{for } -\infty < z < \bar{\eta}(\xi), -\infty < \xi < +\infty \tag{A.1}$$

for solitary-wave solutions, $\bar{\phi}(\xi, z)$, and $\bar{\eta}(\xi)$, where $\xi = x - Vt$, with the boundary conditions

$$0 = \left(-V + \bar{\phi}_\xi\right)\bar{\eta}_\xi - \bar{\phi}_z, \tag{A.2a}$$

$$0 = \frac{1}{2}\left\{\left(-V + \bar{\phi}_\xi\right)^2 + \bar{\phi}_z^2 - V^2\right\} + \bar{\eta} - \frac{\bar{\eta}_{\xi\xi}}{\left(1 + \bar{\eta}_\xi^2\right)^{\frac{3}{2}}} \tag{A.2b}$$

at the free surface $z = \bar{\eta}(\xi)$. (A.2a) is the kinematic boundary condition, which explains that the deformation of the free surface is exactly owing to the normal velocity component of fluid particles on the free surface. (A.2b) is the dynamic boundary condition, explaining the normal stress balance, meaning that the momentum of the fluid is driven by the gravitational acceleration and the surface tension on the free surface.

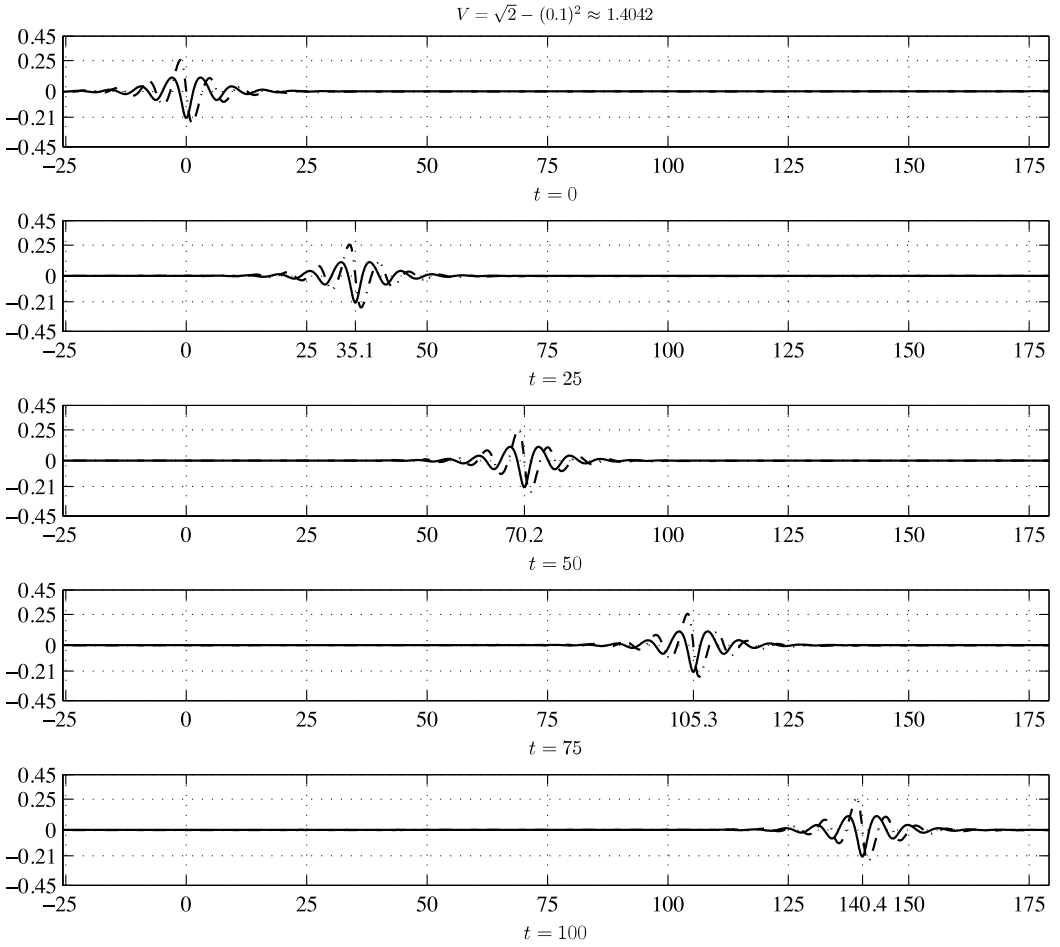

Fig. 6. The unsteady numerical computation of the cubic-order truncation model, with the weakly nonlinear gravity–capillary solitary waves $\eta(x, t)$ $(-)$ and $\zeta(x, t)$ $(--)$ for $V = \sqrt{2} - 0.01$, computed in Fig. 2, as the initial condition. The explicit fourth-order Runge–Kutta method is used on the basis of Fourier spectral method with the discretization parameters $\Delta t = 0.005$ and $\Delta x = 0.1$. The solitary-wave profiles are stably maintained.

Let us define

$$\Phi(\xi, z) \equiv V\xi - \bar{\phi}(\xi, z), \tag{A.3}$$

and $\Psi(\xi, z)$ as a harmonic conjugate of $\Phi(\xi, z)$ such that $\Phi + i\Psi$ is analytic with respect to $\xi + iz$. Then, the following Cauchy–Riemann equations should be satisfied:

$$\Phi_\xi = V - \bar{\phi}_\xi = \Psi_z, \qquad \Psi_\xi = -\Phi_z = \bar{\phi}_z. \tag{A.4}$$

Along the free surface, we have $z = \bar{\eta}(\xi)$, $\Psi \equiv \text{const.} = \Psi_0$, because

$$\left.\frac{\mathrm{d}\Psi}{\mathrm{d}\xi}\right|_{z=\bar{\eta}(\xi)} = \Psi_\xi + \bar{\eta}_\xi \Psi_z = \bar{\phi}_z + \left(V - \bar{\phi}_\xi\right)\bar{\eta}_\xi = 0. \tag{A.5}$$

Since $\Phi + i\Psi$ is analytic with respect to $\xi + iz$, $\xi + iz$ is analytic, as its inverse, with respect to $\Phi + i\Psi$, and so is $\left(\xi_\Phi - \frac{1}{V}\right) + iz_\Phi$. Therefore, from Cauchy's integral formula, we have

$$\left(\xi_\Phi - \frac{1}{V}\right) + iz_\Phi = \frac{i}{\pi}\int_{-\infty}^{+\infty} \frac{\left(\xi_s - \frac{1}{V}\right) + iz_s}{s - \Phi}\mathrm{d}s. \tag{A.6}$$

The factor on the right-hand side of (A.6) is $\frac{1}{\pi i}$, rather than $\frac{1}{2\pi i}$, because it is evaluated on the boundary of the domain. The negative sign comes out of the orientation of the contour integration. Accordingly, we have the following Hilbert transform pair:

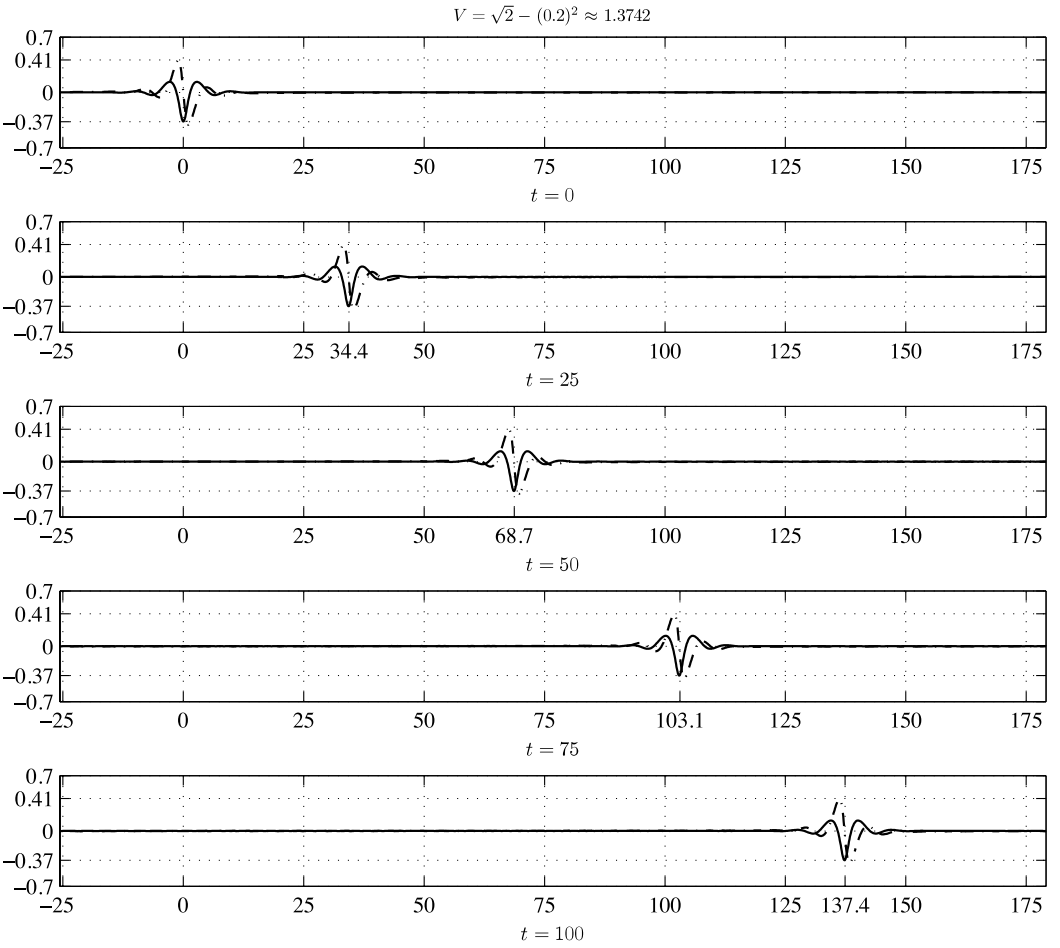

Fig. 7. The unsteady numerical computation of the cubic-order truncation model, with the weakly nonlinear gravity–capillary solitary waves $\eta(x, t)$ $(-)$ and $\zeta(x, t)$ $(--)$ for $V = \sqrt{2} - 0.04$, computed in Fig. 3, as the initial condition. The same method and parameters are used as in Fig. 6.

$$\xi_\Phi - \frac{1}{V} = \frac{1}{\pi}\int_{-\infty}^{+\infty} \frac{z_s}{\Phi - s}\mathrm{d}s = \mathcal{H}\{z_\Phi\} = \bar{G}_0\{z\}, \tag{A.7a}$$

$$z_\Phi = -\frac{1}{\pi}\int_{-\infty}^{+\infty} \frac{\xi_s - \frac{1}{V}}{\Phi - s}\mathrm{d}s = -\mathcal{H}\{\xi_\Phi\} = -\bar{G}_0\{\xi\}, \tag{A.7b}$$

where $\bar{G}_0$ is the one-dimensional counterpart of the operator G, as defined in (8), which corresponds to the derivative of the Hilbert transformation.

It is required that both $\xi_\Phi - \frac{1}{V}$ and z are smooth and vanish as $|\Phi|$ goes to infinity. The kinematic boundary condition has been used in (A.5) in order to derive the Cauchy integral expression up to this point. In fact, the two expressions in (A.7a) and in (A.7b) are equivalent, although not in general, because they are also the harmonic conjugates of each other. That is,

$$\xi_\Phi - \frac{1}{V} = -\mathcal{H}\{\mathcal{H}\{\xi_\Phi\}\} \quad \text{or} \quad z = -\mathcal{H}\{\mathcal{H}\{z\}\} \tag{A.8}$$

does not give any additional information: it only states that ξ and z satisfy Laplace's equation with respect to (Φ, Ψ) in the lower half infinite plane for $-\infty < \Phi < +\infty$ and $-\infty < \Psi < 0$. The description of the full Euler equations is completed together with the dynamic boundary condition.

Now we want to express the dynamic boundary condition in terms of ξ and z, replacing the original variables, $\bar{\eta}$ and $\bar{\phi}$, at the free surface $z = \bar{\eta}(\xi)$. From analyticity, it is evident that

$$\Phi_\xi + i\Psi_\xi = \frac{1}{\xi_\Phi + iz_\Phi} = \frac{\xi_\Phi - iz_\Phi}{\xi_\Phi^2 + z_\Phi^2}, \tag{A.9}$$

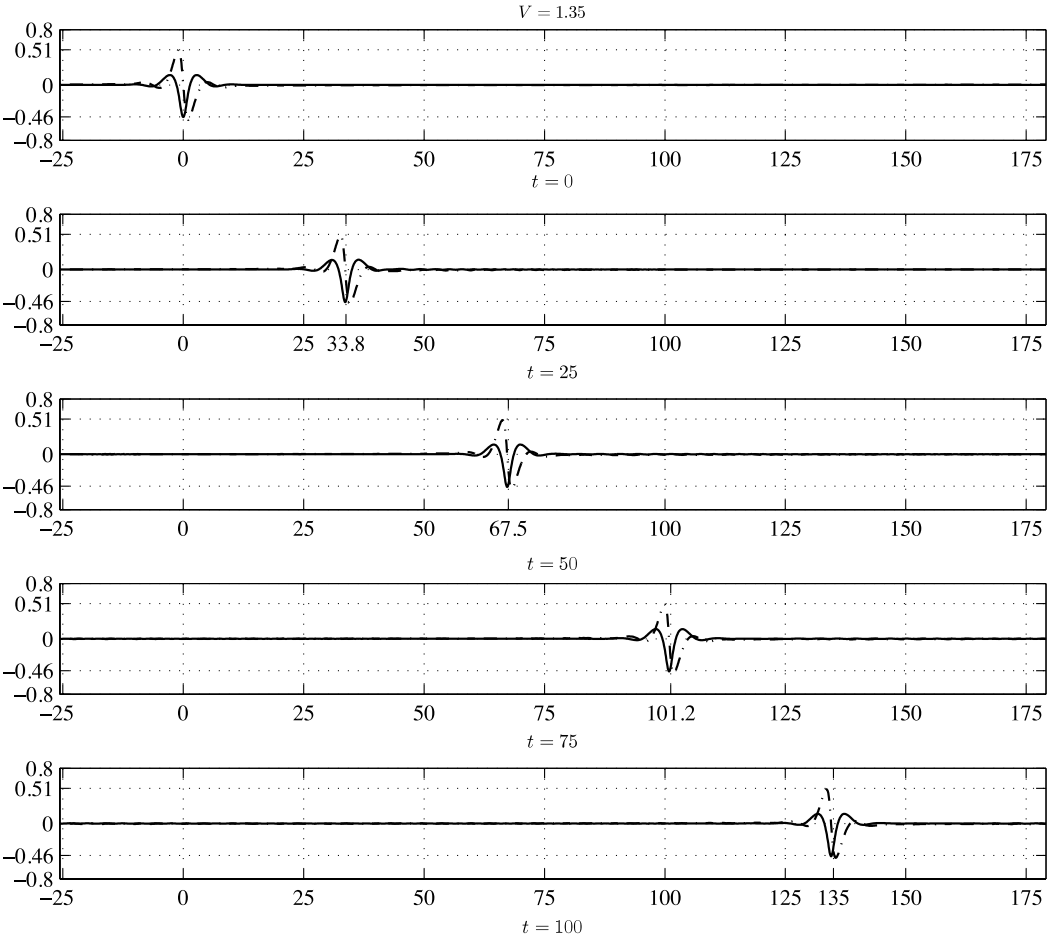

Fig. 8. The unsteady numerical computation of the cubic-order truncation model, with the weakly nonlinear gravity–capillary solitary wave for $V = 1.35$, computed in Fig. 4, as the initial condition. The same method and parameters are used as in Figs. 6 and 7.

thus,

$$V - \bar{\phi}_\xi = \Phi_\xi = \frac{\xi_\Phi}{\xi_\Phi^2 + z_\Phi^2}, \qquad \bar{\phi}_z = \Psi_\xi = -\frac{z_\Phi}{\xi_\Phi^2 + z_\Phi^2}. \tag{A.10}$$

Alternative expressions are introduced for the left-hand sides in (A.7a) in terms of $\bar{\eta}$ and $\bar{\phi}$. Using the chain rule, we have

$$\begin{pmatrix} \Phi_z & \Psi_z \\ \Psi_z & -\Phi_z \end{pmatrix} \begin{pmatrix} z_\Phi \\ z_\Psi \end{pmatrix} = \begin{pmatrix} 1 \\ 0 \end{pmatrix}. \tag{A.11}$$

Hence,

$$z_\Phi = \frac{\Phi_z}{\Phi_z^2 + \Psi_z^2} = \frac{-\bar{\phi}_z}{\bar{\phi}_z^2 + \left(V - \bar{\phi}_\xi\right)^2} = \frac{-\Psi_\xi}{\Phi_\xi^2 + \Psi_\xi^2} = -\xi_\Psi, \tag{A.12a}$$

$$z_\Psi = \frac{\Psi_z}{\Phi_z^2 + \Psi_z^2} = \frac{V - \bar{\phi}_\xi}{\bar{\phi}_z^2 + \left(V - \bar{\phi}_\xi\right)^2} = \frac{\Phi_\xi}{\Phi_\xi^2 + \Psi_\xi^2} = \xi_\Phi. \tag{A.12b}$$

Using the above properties, along the free surface $z = \bar{\eta}(\xi)$, we have

$$\bar{\eta}_\xi = \left.\frac{z_\Phi}{\xi_\Phi}\right|_{z=\bar{\eta}(\xi)}, \qquad \bar{\eta}_{\xi\xi} = \frac{z_{\Phi\Phi}\xi_\Phi - \xi_{\Phi\Phi} z_\Phi}{{\xi_\Phi}^3}. \tag{A.13}$$

Therefore the surface tension term can be expressed by

$$\frac{\bar{\eta}_{\xi\xi}}{\left(1 + \bar{\eta}_\xi^2\right)^{\frac{3}{2}}} = \frac{z_{\Phi\Phi}\xi_\Phi - \xi_{\Phi\Phi} z_\Phi}{{\xi_\Phi}^3} \cdot \frac{1}{\left\{1 + \left(\frac{z_\Phi}{\xi_\Phi}\right)^2\right\}^{\frac{3}{2}}} = \frac{z_{\Phi\Phi}\xi_\Phi - \xi_{\Phi\Phi} z_\Phi}{\left({\xi_\Phi}^2 + {z_\Phi}^2\right)^{\frac{3}{2}}}. \tag{A.14}$$

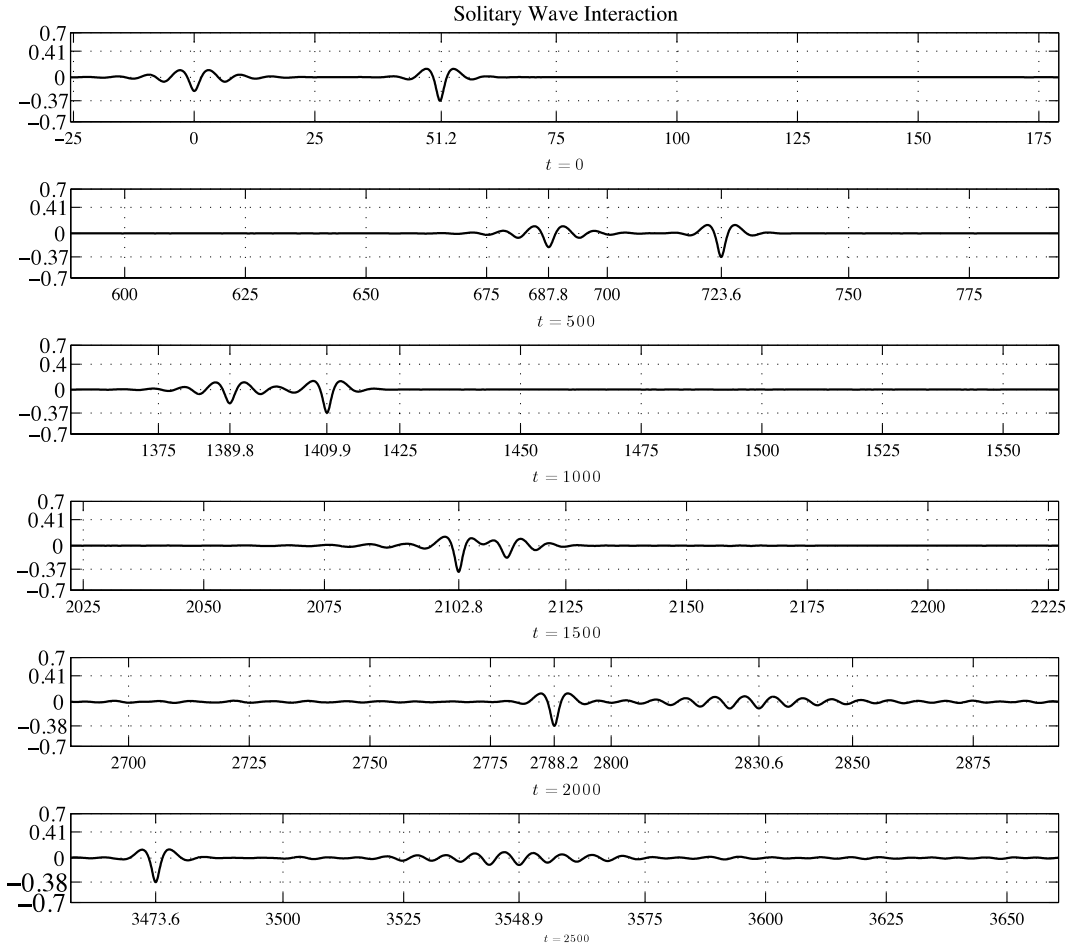

Fig. 9. An interaction between two solitary waves, computed in Figs. 6 and 7, of which wave speeds are $V = \sqrt{2} - 0.01 \approx 1.4042$ (left) and $V = \sqrt{2} - 0.04 \approx 1.3742$ (right), respectively (the surface elevation only). The same method is used with a smaller time step $\Delta t = 0.001$ and the same spatial discretization size and $\Delta x = 0.1$ for $t = 2000$. The smaller solitary wave catches up with the larger one and passes through it. After the collision, the larger one becomes slightly larger and is slowed down to $V \approx 1.3708$ and the smaller one spreads out.

Finally, the dynamic boundary condition is given by

$$0 = \frac{1}{2}\left(\frac{1}{{\xi_\Phi}^2 + {z_\Phi}^2} - V^2\right) + z - \frac{z_{\Phi\Phi}\xi_\Phi - \xi_{\Phi\Phi}z_\Phi}{\left({\xi_\Phi}^2 + {z_\Phi}^2\right)^{\frac{3}{2}}}. \tag{A.15}$$

For numerical implementation, it is convenient to introduce $\chi = \xi_\Phi - \frac{1}{V}$ because it decays to zero at infinity:

$$0 = -\frac{V\chi + \frac{1}{2}V^2\left(\chi^2 + {z_\Phi}^2\right)}{\left(\chi + \frac{1}{V}\right)^2 + {z_\Phi}^2} + z - \frac{\left(\chi + \frac{1}{V}\right)z_{\Phi\Phi} - \chi_\Phi z_\Phi}{\left\{\left(\chi + \frac{1}{V}\right)^2 + {z_\Phi}^2\right\}^{\frac{3}{2}}}. \tag{A.16}$$

Equivalently, a single nonlinear integro–differential equation is reached for $z(\Phi)$:

$$\begin{aligned} 0 = {} & \frac{1}{2}\sqrt{\left(\mathcal{H}\{z_\Phi\} + \frac{1}{V}\right)^2 + {z_\Phi}^2} + \left(z - \frac{1}{2}V^2\right)\left\{\left(\mathcal{H}\{z_\Phi\} + \frac{1}{V}\right)^2 + {z_\Phi}^2\right\}^{\frac{3}{2}} \\ & - \left(\mathcal{H}\{z_\Phi\} + \frac{1}{V}\right)z_{\Phi\Phi} + \mathcal{H}\{z_{\Phi\Phi}\}z_\Phi \end{aligned} \tag{A.17}$$

for $-\infty < \Phi < +\infty$, where $|z(\Phi)| \to 0$ as $|\Phi| \to +\infty$.

Appendix B. Spectrally accurate numerical conversion to the functions of spatial variables $(\Phi, \Psi) \longrightarrow (\xi, z)$

When solitary-wave solutions are computed as the functions of Φ for $-\infty < \Phi < +\infty$ at the free surface $z = \bar{\eta}$ (at $\Psi = 0$), it is natural to convert the solutions as the functions of ξ for $-\infty < \xi < +\infty$.

The main idea is to identify the values of the solutions at a given spatial discretization point ξ_j for $1 \le j \le N$. To this end, the initial value problem of the following first-order ordinary differential equation is solved:

$$\left.\frac{\mathrm{d}\bar{\phi}}{\mathrm{d}\xi}\right|_{z=\bar{\eta}} = \left.\frac{V\chi(\Phi)}{\chi(\Phi)+\frac{1}{V}}\right|_{z=\bar{\eta}} = \left.\frac{V\chi(V\xi-\bar{\phi})}{\chi(V\xi-\bar{\phi})+\frac{1}{V}}\right|_{z=\bar{\eta}} \tag{B.1}$$

for $\bar{\phi}|_{(\xi,z)=(0,\bar{\eta})} = 0$. And then, $\bar{\phi}_j$ for $1 \le j \le N$ can be computed for arbitrary discretization points for ξ. Therefore solitary-wave solutions in terms of ξ along the free surface $z = \bar{\eta}$ are simply recovered by

$$\bar{\eta}|_{\Phi=V\xi_j-\bar{\phi}_j}, \qquad \bar{\chi}|_{\Phi=V\xi_j-\bar{\phi}_j} \quad \text{for } 1 \le j \le N \tag{B.2}$$

along the free surface $\Psi \equiv 0$.

Once the boundary values are converted, in the bulk of fluid flow, for $-\infty < \Phi < +\infty$ and $-\infty < \Psi < 0$, χ and z_Φ are obtained by solving the Dirichlet problem of Laplace's equation, respectively.

References

[1] M.S. Longuet-Higgins, Limiting forms for capillary–gravity waves, J. Fluid Mech. 194 (1988) 351–375.
[2] M.S. Longuet-Higgins, Capillary–gravity waves of solitary type on deep water, J. Fluid Mech. 200 (1989) 451–470.
[3] J.-M. Vanden-Broeck, F. Dias, Gravity–capillary solitary waves in water of infinite depth and related free-surface flows, J. Fluid Mech. 240 (1992) 549–557.
[4] M.S. Longuet-Higgins, Capillary–gravity waves of solitary type and envelope solitons on deep water, J. Fluid Mech. 252 (1993) 703–711.
[5] T.R. Akylas, Envelope solitons with stationary crests, Phys. Fluids 5 (1993) 789–791.
[6] F. Dias, G. Iooss, Capillary–gravity solitary waves with damped oscillations, Physica D 65 (1993) 399–423.
[7] F. Dias, D. Menasce, J.-M. Vanden-Broeck, Numerical study of capillary–gravity solitary waves, Eur. J. Mech B-Fluid 15 (1996) 17–36.
[8] O. Laget, F. Dias, Numerical computation of capillary–gravity interfacial solitary waves, J. Fluid Mech. 349 (1997) 221–251.
[9] D.C. Calvo, T.R. Akylas, Stability of steep gravity–capillary solitary waves in deep water, J. Fluid Mech. 452 (2002) 123–143.
[10] X. Zhang, Capillary–gravity and capillary waves generated in a wind wave tank: observations and theories, J. Fluid Mech. 289 (1995) 51–82.
[11] M.S. Longuet-Higgins, X. Zhang, Experiments on capillary–gravity waves of solitary type on deep water, Phys. Fluids 9 (1997) 1963–1968.
[12] X. Zhang, Observations on waveforms of capillary and gravity–capillary waves, Eur. J. Mech. B-Fluid 18 (1999) 373–388.
[13] E. Părău, J.-M. Vanden-Broeck, M.J. Cooker, Nonlinear three-dimensional gravity–capillary solitary waves, J. Fluid Mech. 536 (2005) 99–105.
[14] E. Părău, J.-M. Vanden-Broeck, M.J. Cooker, Three-dimensional gravity–capillary solitary waves in water of finite depth and related problems, Phys. Fluids 17 (2005) 122101.
[15] P.A. Milewski, Three-dimensional localized solitary gravity–capillary waves, Commun. Math. Sci. 3 (2005) 89–99.
[16] W. Craig, Non-existence of solitary water waves in three dimensions, Philos. T. Roy. Soc. A 360 (2002) 2127–2135.
[17] B. Kim, T.R. Akylas, On gravity–capillary lumps, J. Fluid Mech. 540 (2005) 337–351.
[18] V.D. Djordjevic, L.G. Redekopp, On two-dimensional packets of capillary–gravity waves, J. Fluid Mech. 79 (1977) 703–714.
[19] M.J. Ablowitz, H. Segur, On the evolution of packets of water waves, J. Fluid Mech. 92 (1979) 691–715.
[20] T.R. Akylas, F. Dias, R.H.J. Grimshaw, The effect of the induced mean flow on solitary waves in deep water, J. Fluid Mech. 355 (1998) 317–328.
[21] B. Kim, T.R. Akylas, Transverse instability of gravity–capillary solitary waves, J. Eng. Math. 58 (2007) 167–175.
[22] T. Kataoka, M. Tsutahara, Instability of solitary wave solutions to long-wavelength transverse perturbations in the generalized Kadomtsev–Petviashvili equation with negative dispersion, Phys. Rev. E 70 (2004) 016604.
[23] T. Kataoka, M. Tsutahara, Transverse instability of surface solitary waves, J. Fluid Mech. 512 (2004) 211–221.
[24] T. Kataoka, The stability of finite-amplitude interfacial solitary wave, Fluid Dyn. Res. 38 (2006) 831–867.
[25] T. Kataoka, Transverse instability of interfacial solitary waves, J. Fluid Mech. 611 (2008) 255–282.
[26] B. Kim, T.R. Akylas, On gravity–capillary lumps, part 2, two-dimensional Benjamin equation, J. Fluid Mech. 557 (2006) 237–256.
[27] B. Kim, Long-wave transverse instability of interfacial gravity–capillary solitary waves in a two-layer potential flow in deep water, J. Eng. Math. 65 (2009) 325–344.
[28] T.J. Bridges, Transverse instability of solitary-wave states of the water-wave problem, J. Fluid Mech. 439 (2001) 255–278.
[29] B. Akers, P.A. Milewski, A model equation for wavepacket solitary waves arising from capillary–gravity flows, Stud. Appl. Math. 122 (2009) 249–274.
[30] B. Akers, P.A. Milewski, Dynamics of three-dimensional gravity–capillary solitary waves in deep water, SIAM J. Appl. Math. 70 (2010) 2390–2408.
[31] P.A. Milewski, J.-M. Vanden-Broeck, Z. Wang, Dynamics of steep two-dimensional gravity–capillary solitary waves, J. Fluid Mech. 664 (2010) 466–477.
[32] E. Părău, J.-M. Vanden-Broeck, M.J. Cooker, Time evolution of three-dimensional nonlinear gravity–capillary free-surface flows, J. Eng. Math. 68 (2010) 291–300.
[33] V.E. Zakharov, Stability of periodic waves of finite amplitude on the surface of a deep fluid, J. Appl. Mech. Tech. Phys. 9 (1968) 190–194.
[34] A.I. Dyachenko, A.O. Korotkevich, V.E. Zakharov, Weak turbulent Kolmogorov spectrum for surface gravity waves, Phys. Rev. Lett. 92 (2004) 134501.
[35] A.P. Calderón, Cauchy integrals on Lipschitz curves and related operator, Proc. Natl. Acad. Sci. USA 74 (1977) 1324–1327.
[36] R.R. Coifman, Y. Meyer, Nonlinear harmonic analysis and analytic dependence, P. Symp. Pure Math. 43 (1985) 71–78.
[37] W. Craig, C. Sulem, Numerical simulation of gravity waves, J. Comput. Phys. 108 (1993) 73–83.
[38] D.P. Nicholls, Traveling water waves: spectral continuation methods with parallel implementation, J. Comput. Phys. 143 (1998) 224–240.
[39] D.P. Nicholls, On hexagonal gravity water waves, Math. Comput. Simul. 55 (2001) 567–575.
[40] W. Craig, D.P. Nicholls, Traveling gravity water waves in two and three dimensions, Eur. J. Mech. B-Fluids 21 (2002) 615–641.
[41] W. Artiles, A. Nachbin, Asymptotic nonlinear wave modeling through the Dirichlet-to-Neumann operator, Methods Appl. Anal. 11 (2004) 475–492.
[42] P. Guyenne, D.P. Nicholls, Numerical simulation of solitary waves on plane slopes, Math. Comput. Simul. 69 (2005) 269–281.
[43] D.P. Nicholls, M. Taber, Detection of ocean bathymetry from surface wave measurements, Eur. J. Mech. B-Fluid 28 (2009) 224–233.
[44] D.P. Nicholls, F. Reitich, A new approach to analyticity of Dirichlet–Neumann operators, P. Roy. Soc. Edinburgh A 131 (2001) 1411–1433.
[45] D.P. Nicholls, F. Reitich, Stability of high-order perturbative methods for the computation of Dirichlet–Neumann operators, J. Comput. Phys. 170 (2001) 276–298.
[46] D.P. Nicholls, F. Reitich, On analyticity of traveling water waves, Proc. R. Soc. A 461 (2005) 1283–1309.
[47] D.P. Nicholls, F. Reitich, Stable, high-order computation of traveling water waves in three dimensions, Eur. J. Mech. B-Fluid 25 (2006) 406–424.

[48] D.P. Nicholls, M. Taber, Joint analyticity and analytic continuation of Dirichlet–Neumann operators on doubly perturbed domains, J. Math. Fluid Mech. 10 (2008) 238–271.
[49] D.P. Nicholls, F. Reitich, Analytic continuation of Dirichlet–Neumann operator, Numer. Math. 94 (2003) 107–146.
[50] D.P. Nicholls, Boundary perturbation methods for water waves, GAMM-Mitteilungen 30 (2007) 44–74.
[51] B. West, K.A. Brueckner, R.S. Janda, D.M. Milder, R.L. Milton, A new numerical method for surface hydrodynamics, J. Geophys. Res. 92 (1987) 11803–11824.
[52] D.G. Dommermuth, D.K.P. Yue, A high-order spectral method for the study of nonlinear gravity waves, J. Fluid Mech. 184 (1987) 267–288.
[53] D.S. Agafontsev, F. Dias, E.A. Kuznetsov, Deep-water internal solitary waves near critical density ratio, Physica D 225 (2007) 153–168.
[54] D.J. Benney, A.C. Newell, The propagation of nonlinear wave envelopes, J. Math. Phys. 46 (1967) 133–139.
[55] H. Hasimoto, H. Ono, Nonlinear modulation of gravity waves, J. Phys. Soc. Japan 33 (1972) 805–811.
[56] A. Davey, K. Stewartson, On three-dimensional packets of surface waves, Proc. R. Soc. Lond. A 338 (1974) 101–110.
[57] D.J. Benney, G.J. Roskes, Wave instabilities, Stud. Appl. Math. 48 (1969) 377–385.
[58] W. Craig, C. Sulem, P.L. Sulem, Nonlinear modulation of gravity waves: a rigorous approach, Nonlinearity 5 (1992) 497–522.
[59] W. Craig, U. Schanz, C. Sulem, The modulational regime of three-dimensional water waves and the Davey–Stewartson system, Ann. I. H. Poincare-An. 14 (1997) 615–667.
[60] S.J. Hogan, The fourth-order evolution equation for deep-water gravity–capillary waves, Proc. R. Soc. Lond. A 402 (1985) 359–372.
[61] F. Dias, C. Kharif, Nonlinear gravity and capillary–gravity waves, Annu. Rev. Fluid Mech. 31 (1999) 301–346.
[62] P.A. Milewski, E. Tabak, A pseudo-spectral procedure for the solution of nonlinear wave equations with examples from free-surface flows, SIAM J. Sci. Comput. 21 (1999) 1102–1114.
[63] B. Kim, Long-wave transverse instability of weakly nonlinear gravity–capillary solitary waves, J. Eng. Math. (in press).
[64] D.C. Calvo, T.R. Akylas, On interfacial gravity–capillary solitary waves of the Benjamin type and their stability, Phys. Fluids 15 (2003) 1261–1270.
[65] M.S. Longuet-Higgins, On the mass, momentum, energy and circulation of a solitary wave, Proc. R. Soc. Lond. A 337 (1974) 1–13.
[66] M.S. Longuet-Higgins, J.D. Fenton, On the mass, momentum, energy and circulation of a solitary wave, II, Proc. R. Soc. Lond. A 340 (1974) 471–493.